Electromagnetically Induced Transparency Cooling of High-Nuclear-Spin Ions

Chuanxin Huang,[1,*] Chenxi Wang,[1,*] Hongxuan Zhang,[1] Hongyuan Hu,[1] Zuqing Wang,[1] Zhichao Mao,[2] Shijiao Li,[1] Panyu Hou,[1,3] Yukai Wu,[1,3] Zichao Zhou,[1,3,†] and Luming Duan[1,3,4,‡]

[1]*Center for Quantum Information, Institute for Interdisciplinary Information Sciences, Tsinghua University, Beijing 100084, People's Republic of China*

[2]*HYQ Co., Ltd., Beijing 100176, People's Republic of China*

[3]*Hefei National Laboratory, Hefei 230088, People's Republic of China*

[4]*New Cornerstone Science Laboratory, Beijing 100084, People's Republic of China*

(Received 30 April 2024; accepted 26 August 2024; published 13 September 2024)

We report the electromagnetically induced transparency (EIT) cooling of $^{137}Ba^{+}$ ions with a nuclear spin of $I = 3/2$, which are a good candidate of qubits for future large-scale trapped-ion quantum computing. EIT cooling of atoms or ions with a complex ground-state level structure is challenging due to the lack of an isolated Λ system, as the population can escape from the Λ system to reduce the cooling efficiency. We overcome this issue by leveraging an EIT pumping laser to repopulate the cooling subspace, ensuring continuous and effective EIT cooling. We cool the two radial modes of a single $^{137}Ba^{+}$ ion to average motional occupations of 0.08(5) and 0.15(7), respectively. Using the same laser parameters, we also cool all the ten radial modes of a five-ion chain to near their ground states. Our approach can be adapted to atomic species possessing similar level structures. It allows engineering of the EIT Fano-like spectrum, which can be useful for simultaneous cooling of modes across a wide frequency range, aiding in large-scale trapped-ion quantum information processing.

DOI: 10.1103/PhysRevLett.133.113204

Trapped ions are a powerful and versatile platform, enabling a broad range of research in quantum information processing (QIP) [1,2], precision spectroscopy [3], and tests of fundamental physics [4]. Ions can be controlled by laser and microwave fields, and can achieve high-fidelity operations including state preparation and measurement [5–10], single-qubit gates [5,11], and two-qubit gates [12–15], for up to tens of ions [10,16–18]. Hundreds of ions have also been used for quantum simulation in Paul traps [19] and Penning traps [20,21].

For laser-based gate operations, thermal motion of ions causes random fluctuation in laser phase and intensity, fundamentally limiting gate fidelity. Although advanced techniques such as the widely used Molmer-Sorensen entangling gate [22,23] alleviate the requirement of ground-state cooling, it is still desirable to cool the relevant motional modes of ions to the lowest possible temperature for achieving high-fidelity QIP. Among the common sub-Doppler cooling methods, resolved sideband cooling has been routinely applied to small ion crystals, typically achieving an average motional qunatum (phonon) number $\bar{n} < 0.1$ [24,25]. However, due to the narrow cooling band, its cooling time generally grows with the number of ions [26,27], which is inefficient for large ion crystals. Polarization gradient cooling [28–30] offers a broader cooling band, but the attainable $\bar{n} \approx 1$ is high [31]. In contrast, electromagnetically induced transparency (EIT) cooling [25,32] provides high cooling rates and broad cooling bandwidth, while maintaining a low cooling limit $\bar{n} \approx 0.1$, making it a suitable cooling method for quantum computing [33] and quantum simulation [2] with large ion crystals.

EIT cooling has been demonstrated with ions that have a relatively simple level structure including $^{24}Mg^{+}$ [34] and $^{40}Ca^{+}$ [35,36] with no nuclear spins, and $^{171}Yb^{+}$ with a nuclear spin $I = 1/2$ [37,38]. It has also been realized with $^{9}Be^{+}$ possessing $I = 3/2$ but under a strong magnetic field (4.46 T) [39], such that only electron spin states are relevant. However, for ions with high nuclear spins $I > 1/2$ at a low or intermediate magnetic field, EIT cooling is challenging due to the difficulty of finding an isolated Λ level structure. Despite this difficulty, many high-nuclear-spin ion species such as $^{9}Be^{+}$, $^{25}Mg^{+}$, and $^{43}Ca^{+}$ have been widely used for QIP due to their long coherence times and high-fidelity quantum operations [9,12,13,40–43]. In particular, $^{137}Ba^{+}$ ions with $I = 3/2$ recently have attracted increasing interest due to the required laser transitions in the visible wavelength range [9,40,43]. This provides key benefits for large-scale QIP, as high laser power is more accessible at this range and these lasers cause less photo-induced charging [44] and damage in optics compared to

*These authors contributed equally to this work.

†Contact author: zichaozhou@mail.tsinghua.edu.cn

‡Contact author: lmduan@tsinghua.edu.cn

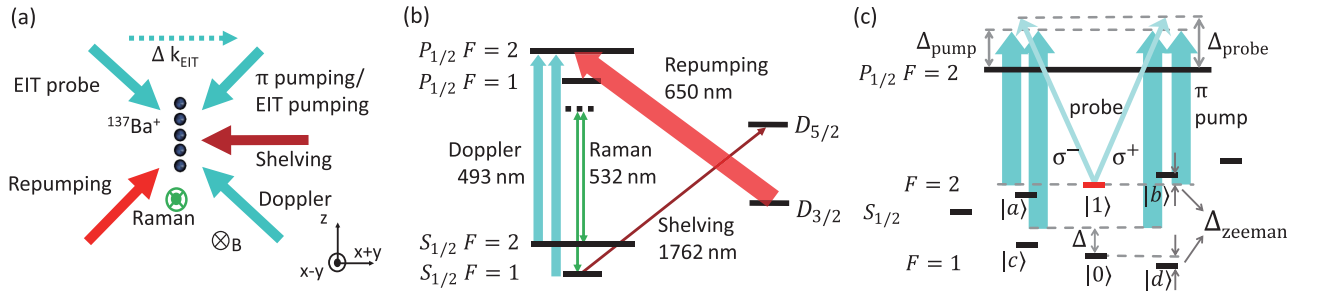

FIG. 1. (a) Experiment configuration and (b) relevant energy levels of $^{137}Ba^{+}$ ions. We use 493 nm lasers for Doppler and EIT cooling. A 650 nm laser repumps the population in the $D_{3/2}$ level to the $P_{1/2}$ level. A 1762 nm laser transfers the population in $|0\rangle$ [see (c)] to $D_{5/2}$ for state readout. A pair of focused 532 nm Raman laser beams are use to drive sideband transitions for measuring average phonon numbers. (c) Relevant energy levels and laser couplings of the EIT cooling scheme. A weak probe beam (narrow cyan arrows) has σ_+ and σ_- polarization components. A strong π-polarized pump beam (broad cyan arrows) consists of two frequency components separated by approximately the hyperfine splitting of 8.037 GHz. In the limit of weak probe, the ion mostly stays in the $|1\rangle$ state with EIT cooling occurring between this state and the four nearby states $|a\rangle$, $|b\rangle$, $|c\rangle$, and $|d\rangle$.

lasers near or within ultraviolet range used for other ion species mentioned above.

In this Letter, we demonstrate EIT cooling with $^{137}Ba^{+}$ ions. We modify a laser configuration used for qubit state initialization to perform EIT cooling in an open Λ system. Despite all eight states in the ground-state manifold that are involved in the dynamics during EIT cooling, EIT pump beams, which also serve as repumping beams, keep population in the cooling subspace. (See Supplemental Material Sec. V [45] for generalization to other high-nuclear-spin ion species.) We cool two radial modes of a single $^{137}Ba^{+}$ ion to $\bar{n}$ of 0.08(5) and 0.15(7), respectively. By using the same laser parameters, we further cool all radial modes of a five-ion chain to near the ground states.

The experimental system and laser couplings are depicted in Fig. 1. We confine up to five $^{137}Ba^{+}$ ions in a blade trap with trap frequencies $(\omega_x, \omega_y, \omega_z) = 2\pi \times (1.7, 1.8, 0.2)$ MHz. We denote the ion chain axis as z coinciding with the trap axis. A quantization field of approximately 6.7 G is applied perpendicular to the z axis, leading to a Zeeman splitting of $\Delta_{\text{Zeeman}} = 2\pi \times 4.7$ MHz between adjacent $S_{1/2}$ Zeeman levels. A Doppler cooling beam at 493 nm has all the three polarization components and couples to modes in all the three principle axes. It has two frequency components that respectively couple the $S_{1/2}, F = 1$ and $S_{1/2}, F = 2$ states to $P_{1/2}, F = 2$ with a detuning of $-\Gamma/2$, where $\Gamma = 2\pi \times 20.1$ MHz is the natural linewidth of the $P_{1/2}$ states. A π-polarized 493 nm laser, used for optical pumping [π pumping in Fig. 1(a)], also has two frequency components to resonantly couple $S_{1/2}, F = 1, 2$ states to $P_{1/2}, F = 2$, respectively. Owing to the selection rule, the ion will be pumped to the dark state $|1\rangle \equiv |S_{1/2}, F = 2, m_F = 0\rangle$ ideally. This beam also serves as a pump beam in EIT cooling which will be described later. During the cooling and optical pumping cycles, ions can decay to $D_{3/2}$ and remain dark. We use a strong near-resonant 650 nm laser (repumping beam) containing multiple frequency components to deplete the population in all the hyperfine levels in $D_{3/2}$. A pair of counterpropagating 532 nm Raman laser beams can drive Raman sideband transitions between $|0\rangle \equiv |S_{1/2}, F = 1, m_F = 0\rangle$ and $|1\rangle$ for thermometry of ions. Their beam waist radius is approximately 2 μm, which is smaller than the distance between neighboring ions in a chain. To distinguish $|0\rangle$ and $|1\rangle$, we first apply three 1762 nm π pulses to sequentially shelve the population in $|0\rangle$ to three different Zeeman levels in $D_{5/2}$, which can suppress the shelving error from imperfect π pulses [9]. Then, we turn on the Doppler cooling laser with its frequency adjusted to resonance. Ions only fluoresce when in $|1\rangle$ and fluorescence photons are collected by a photomultiplier tube for a single ion or an electron-multiplying CCD for multiple ions. The typical state preparation and measurement error is about 2% dominated by polarization errors in the π pumping beam for state initialization.

As shown in Fig. 1(a), the EIT laser beams consist of a strong pump beam and a weak probe beam. Their wave vector difference $\Delta \boldsymbol{k}_{\text{EIT}}$ is perpendicular to the z axis and has roughly equal projections onto the x and y axes. The π-polarized EIT pump beam is the same beam for optical pumping with its frequency shifted by Δ_{pump} as shown in Fig. 1(c). We denote the Rabi frequencies of its two frequency components by $\Omega_{\text{pump},1(2)}$ according to their coupling to $S_{1/2}, F = 1(2)$ levels, with $\Omega_{\text{pump},2}/\Omega_{\text{pump},1} \approx 2$ controlled by an electro-optic modulator. (See Supplemental Material Sec. III [45] for more details.) Their relative detuning can be adjusted to fine-tune the Fano-like spectrum for optimizing EIT cooling. The probe beam, containing equal σ_+ and σ_- components, couples $|1\rangle$ to the $P_{1/2}, F = 2$ levels with a detuning Δ_{probe} and a Rabi rate Ω_{probe}. Note that the Rabi frequency used here only represents the transition strength between the $S_{1/2}$ and $P_{1/2}$ levels. For the Rabi frequencies between detailed Zeeman levels, the Clebsch-Gordan coefficients should further be multiplied (see Supplemental Material Sec. I).

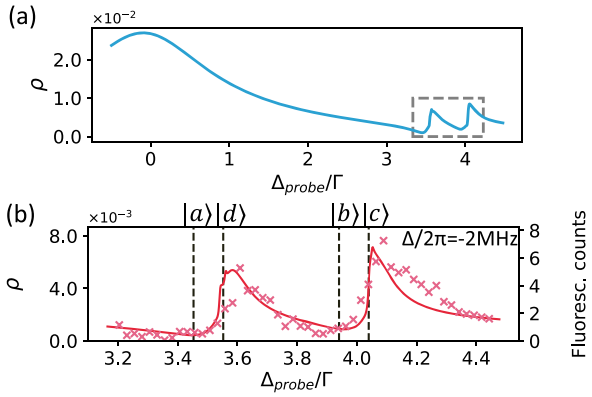

FIG. 2. (a) Fano-like spectrum from numerical simulations when the two frequency components of the EIT pump beam are separated by $\omega_{01} - \Delta$, where ω_{01} is the qubit transition frequency and $\Delta/2\pi = -2$ MHz. The broad peak around $\Delta_{\text{probe}} = 0$ corresponds to the resonance of $|1\rangle \rightarrow |P_{1/2}, F = 2\rangle$. The Fano-like line shapes associated with EIT in the gray box are enlarged in (b) and compared to the experimental spectrum (crossing marks, after subtracting the background of 7.5 photon counts). Vertical dashed lines indicate the dark resonances of four possible Λ systems containing $|1\rangle$ and one of $\{|a\rangle, |b\rangle, |c\rangle, |d\rangle\}$.

EIT cooling scheme—In the limit $\Omega_{\text{probe}} \ll \Omega_{\text{pump},1(2)}, \Gamma$, the steady state when all EIT beams are on is $|1\rangle$. A weak probe beam can lead to some excitation to the $P_{1/2}$ levels. When the dark resonance condition $\Delta_{\text{probe}} = \Delta_{\text{pump}} \pm \Delta_{\text{Zeeman}}$ or $\Delta_{\text{probe}} = \Delta_{\text{pump}} + \Delta \pm \Delta_{\text{Zeeman}}$ is satisfied, we expect coherent population trapping in $|1\rangle$ and one of the four nearby states denoted as $|a\rangle$, $|b\rangle$, $|c\rangle$, and $|d\rangle$, so that the excitation to the $P_{1/2}$ level is suppressed. Fano-like spectra associated with this phenomenon can be observed by tuning the probe beam frequency across the dark resonances, for example, the spectrum shown in Fig. 2(a). Such a Fano-like spectrum can be used to estimate the EIT cooling limit $\bar{n}_f$ and cooling rate γ (in the absence of heating from environment), which are given by [25]

$$\bar{n}_f = \frac{\rho(\Delta_{\text{probe}}) + \rho(\Delta_{\text{probe}} - \omega)}{\rho(\Delta_{\text{probe}} + \omega) - \rho(\Delta_{\text{probe}} - \omega)} \tag{1}$$

and

$$\gamma = \eta^2 \Gamma [\rho(\Delta_{\text{probe}} + \omega) - \rho(\Delta_{\text{probe}} - \omega)], \tag{2}$$

where ρ is the population of the $P_{1/2}$ states, ω is the phonon mode frequency, and η is the Lamb-Dicke parameter of the EIT beams with a wave vector difference $\Delta \boldsymbol{k}_{\text{EIT}}$.

The key difference from ions with $I = 0$ or $1/2$ is that high-nuclear-spin ions have a number of extra ground states and excited states to which ions can escape from the EIT cooling subspace, reducing or diminishing cooling efficacy (see Supplemental Material Sec. IV [45] for more details). In previous works with $^{171}\text{Yb}^+$ ($I = 1/2$) [37,38], the leakage issue was addressed by employing an additional repump laser with the desired ground states protected by the selection rule. However, for $^{137}\text{Ba}^+$, adding repumpers can potentially destroy the ground states used in EIT cooling through their coupling to the extra Zeeman levels of $P_{1/2}$. Here, we design an EIT cooling scheme where the EIT pump laser simultaneously serves as the repump beam to ensure the cooling efficiency.

In Fig. 2 we compute the Fano-like spectrum to guide the design of cooling parameters and compare it with experimental results. In the simulation, we consider all hyperfine states in the $S_{1/2}, F = 1, 2$ and $P_{1/2}, F = 2$ manifolds. The $D_{3/2}$ states are ignored since they are efficiently depleted, and we treat this effect as a reduction of the $P_{1/2}$ spontaneous emission rate $\Gamma = 2\pi \times 20.1$ MHz by multiplying the branching ratio of 0.732 from $P_{1/2}$ to $S_{1/2}$ states [47]. In general, the interplay of multiple energy levels with multiple laser frequency components is solved by a Lindblad master equation with a time-dependent Hamiltonian. Here we simplify the calculation by computing the spectra for the σ^+ and σ^- components of the probe beam separately and add them up together. Then, each spectrum can be obtained efficiently by solving a time-independent Lindblad master equation after going into a suitable rotating frame. This approximation is valid to the first order for a weak probe beam since these two polarization components lead to excitation to Zeeman levels with positive and negative m_F, respectively, with little overlap. Therefore, we expect their spectra to add up incoherently. More details can be found in Supplemental Material Sec. I [45].

Figure 2(a) shows the combined spectrum, which is the total population of the $P_{1/2}, F = 2$ manifold as a function of Δ_{probe}. The calculation uses parameters close to experimental numbers, including $\Omega_{\text{probe},+} = \Omega_{\text{probe},-} = 0.40\Gamma$, $\Omega_{\text{pump},1} = 1.5\Gamma$, $\Omega_{\text{pump},2} = 3.0\Gamma$, $\Delta_{\text{pump}} = 3.7\Gamma$. (See Supplemental Material Sec. II for their calibrations [45].) We choose $\Delta = 2\pi \times -2$ MHz so that the two sets of bright resonant peaks merge together to allow efficient EIT cooling. The Fano-like line shape for the four possible Λ systems is highlighted by the gray box and is further enlarged in Fig. 2(b), where the dark resonances are indicated by the vertical dashed lines and are labeled by the corresponding states. We also experimentally verify this spectrum with a single $^{137}\text{Ba}^+$ ion by turning on the EIT cooling beams for 3 ms and count the scattered photon number which is proportional to the $P_{1/2}$ population. The line shape of the experimental data represented by crossing marks agrees with the computed spectrum. Note that a nonzero background of 7.5 photons has already been subtracted from the measured photon counts.

Cooling of a single ion—We perform EIT cooling with a single ion using the pulse sequence shown in Fig. 3(a). After Doppler cooling, the single ion is EIT cooled for a

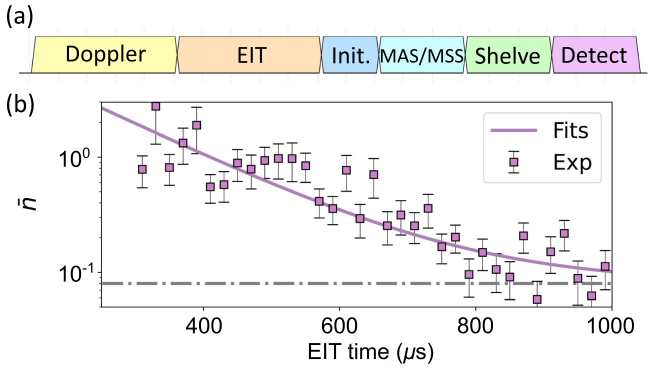

FIG. 3. Single-ion EIT cooling. (a) EIT cooling pulse sequence. After Doppler and EIT cooling, we initialize the qubit state in $|1\rangle$ by optical pumping. Then we apply a motion-adding sideband (MAS) or motion-subtracting sideband (MSS) pulse before shelving detection. (b) EIT cooling dynamics with optimized parameters. We omit the data points for the first 300 μs since they are too high to be measured accurately by sideband ratio method. We fit the data points to $\bar{n}(t) = (\bar{n}_i - \bar{n}_f)\exp(-t/\tau) + \bar{n}_f$, which yields a cooling limit $\bar{n}_f = 0.08(2)$ (horizontal dashed line) and a $1/e$ cooling time $\tau = 0.15(6)$ ms. Error bars represent 1 standard deviation.

certain duration followed by an optical pumping pulse to reset the internal state to $|1\rangle$. Then, we apply a motion-adding sideband (MAS) or motion-subtracting sideband (MSS) π pulse before shelving detection. We estimate $\bar{n}$ by using the ratio of the MAS and MSS excitation probabilities [25].

We set $\Delta_{\text{probe}} = \Delta_{\text{pump}} - \Delta_{\text{Zeeman}} = 3.45\Gamma$ to satisfy the dark resonance condition for the $|1\rangle$ and $|a\rangle$ states. To calibrate the optimal pump beam intensity for given transverse modes, we perform EIT cooling with varying pump beam power for a fixed duration of 2 ms, and measure $\bar{n}$ of the x mode as a metric (see Supplemental Material Sec. III [45]). We determine the optimal values $\Omega_{\text{pump},1} = 2.2\Gamma$ and $\Omega_{\text{pump},2} = 4.4\Gamma$. As for the probe intensity, in the absence of heating from environment, the cooling limit decreases monotonically as decreasing the probe beam intensity. In practice, external heating cannot be neglected and an optimal value of $\Omega_{\text{probe}} = 0.40\Gamma$ is determined from calibration.

Next, we investigate the cooling dynamics by measuring $\bar{n}$ for variable cooling time t and show the experiment results in Fig. 3(b). We fit the experimental data points to an exponential decay $\bar{n}(t) = (\bar{n}_i - \bar{n}_f)\exp(-t/\tau) + \bar{n}_f$, yielding $\tau = 0.15(6)$ ms, $\bar{n}_i = 11.8(2.6)$, and $\bar{n}_f = 0.08(2)$. At a longer duration of 2 ms, the x mode phonon number is measured to be $\bar{n} = 0.08(5)$, consistent with the fitted $\bar{n}_f$. The fitting result corresponds to a measured cooling rate $\gamma = 7(2)$ ms^{-1}, consistent with the theoretical calculation of 7.2 ms^{-1} using Eq. (2). As the x and y modes have similar frequencies, the EIT cooling optimized for the x mode also cools the y mode to an average phonon number of 0.15(7) for a 2 ms cooling duration. The higher $\bar{n}$ of the y mode is primarily from its larger heating rate of 0.8(2) ms^{-1} compared to the 0.10(6) ms^{-1} of the x mode.

Cooling of a multi-ion chain—Finally, we use the same parameters optimized for a single ion to EIT cool a five-ion chain, whose radial modes span a frequency range of about 270 kHz. By using the same experimental sequence in Fig. 3(a), we simultaneously cool all ten radial modes and show the final $\bar{n}$ in Fig. 4(b). Raman pulses for sideband

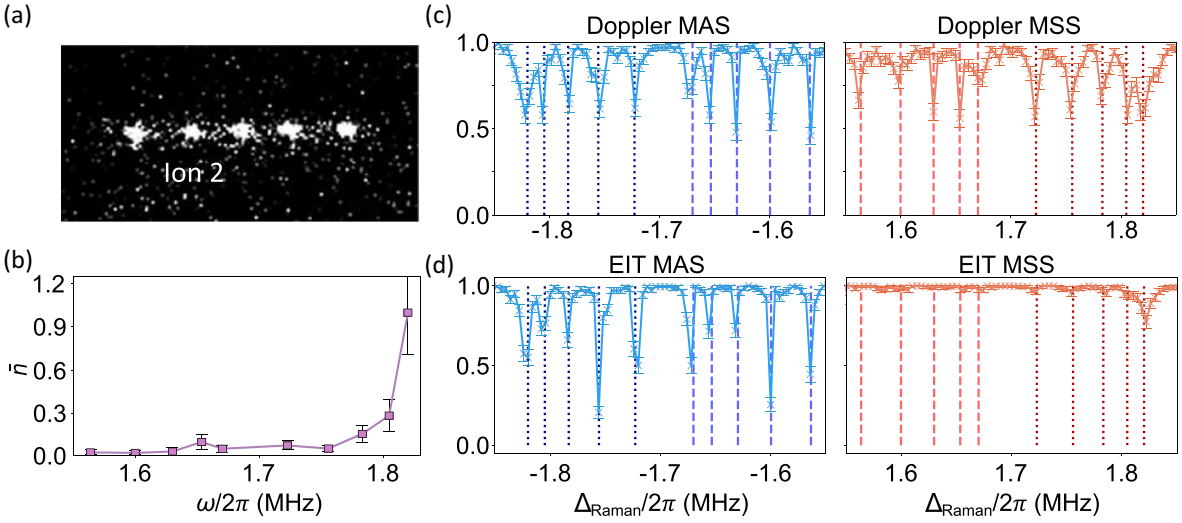

FIG. 4. Simultaneous EIT cooling of a multi-ion chain. (a) Image of a five-ion chain. Ion 2 is selectively addressed by Raman beams for average phonon number measurements. (b) Average phonon number $\bar{n}$ of all the ten radial modes calculated from MAS and MSS excitation probabilities shown in (d). Except for the y center-of-mass mode (the highest frequency mode with the largest heating rate proportional to the ion number), the rest modes are cooled to an average $\bar{n} = 0.09$. (c),(d) MAS and MSS excitation spectra after Doppler cooling (c) and EIT cooling (d). Data points are connected by solid lines to guide the eye. Vertical dashed and dotted lines indicate the frequencies of the x and y modes, respectively. Error bars in (b)–(d) represent 1 standard deviation.

thermometry are only applied to ion 2 [labeled in Fig. 4(a)]. The MAS and MSS spectra after Doppler cooling and after EIT cooling are, respectively, shown in Figs. 4(c) and 4(d). The MSS excitation probabilities after EIT cooling are greatly suppressed for all the radial modes except for the y center-of-mass mode due to its high heating rate proportional to the ion number. This mode is cooled to $\bar{n} = 1.0(3)$, still significantly smaller than the Doppler limit of $\bar{n} \approx 10$. The other nine modes are cooled to much lower $\bar{n}$ with an average number of 0.09.

In summary, we introduce an EIT cooling scheme applicable for atomic species possessing high nuclear spins at low fields. We successfully implement this scheme with both a single $^{137}Ba^{+}$ ion and a five-ion chain, achieving average phonon numbers well below the Doppler cooling limit. Our approach can be extended to other atomic species possessing high nuclear spins and can provide efficient cooling for large ion crystals. More importantly, our scheme indicates that many ground states are not necessarily an issue for EIT cooling, but it offers freedoms to engineer the Fano-like spectrum to optimize cooling for specific scenarios. For example, we can perform simultaneous cooling of both radial and axial modes within different frequency ranges by adjusting the EIT beam propagation directions and tuning laser parameters. More details can be found in Supplemental Material Sec. IV [45].

Note added—Recently, we became aware that the NIST Ion Storage Group is investigating EIT cooling with the $I = 5/2$ $^{25}Mg^{+}$ isotope.

Acknowledgments—This work was supported by Innovation Program for Quantum Science and Technology (2021ZD0301601), Tsinghua University Initiative Scientific Research Program, and the Ministry of Education of China. L. D. acknowledges in addition support from the New Cornerstone Science Foundation through the New Cornerstone Investigator Program. Y. W. acknowledges in addition support from Tsinghua University Dushi program. P. H. acknowledges the start-up fund from Tsinghua University.

[1] C. D. Bruzewicz, J. Chiaverini, R. McConnell, and J. M. Sage, Trapped-ion quantum computing: Progress and challenges, Appl. Phys. Rev. **6**, 021314 (2019).
[2] C. Monroe, W. C. Campbell, L.-M. Duan, Z.-X. Gong, A. V. Gorshkov, P. W. Hess, R. Islam, K. Kim, N. M. Linke, G. Pagano, P. Richerme, C. Senko, and N. Y. Yao, Programmable quantum simulations of spin systems with trapped ions, Rev. Mod. Phys. **93**, 025001 (2021).
[3] A. D. Ludlow, M. M. Boyd, J. Ye, E. Peik, and P. O. Schmidt, Optical atomic clocks, Rev. Mod. Phys. **87**, 637 (2015).
[4] M. S. Safronova, D. Budker, D. DeMille, Derek F. Jackson Kimball, A. Derevianko, and C. W. Clark, Search for new physics with atoms and molecules, Rev. Mod. Phys. **90**, 025008 (2018).
[5] T. P. Harty, D. T. C. Allcock, C. J. Ballance, L. Guidoni, H. A. Janacek, N. M. Linke, D. N. Stacey, and D. M. Lucas, High-fidelity preparation, gates, memory, and readout of a trapped-ion quantum bit, Phys. Rev. Lett. **113**, 220501 (2014).
[6] J. E. Christensen, D. Hucul, W. C. Campbell, and E. R. Hudson, High-fidelity manipulation of a qubit enabled by a manufactured nucleus, npj Quantum Inf. **6**, 35 (2020).
[7] A. Ransford, C. Roman, T. Dellaert, P. McMillin, and W. C. Campbell, Weak dissipation for high-fidelity qubit-state preparation and measurement, Phys. Rev. A **104**, L060402 (2021).
[8] S. D. Erickson, J. J. Wu, P.-Y. Hou, D. C. Cole, S. Geller, A. Kwiatkowski, S. Glancy, E. Knill, D. H. Slichter, A. C. Wilson, and D. Leibfried, High-fidelity indirect readout of trapped-ion hyperfine qubits, Phys. Rev. Lett. **128**, 160503 (2022).
[9] F. A. An, A. Ransford, A. Schaffer, L. R. Sletten, J. Gaebler, J. Hostetter, and G. Vittorini, High fidelity state preparation and measurement of ion hyperfine qubits with $I > \frac{1}{2}$, Phys. Rev. Lett. **129**, 130501 (2022).
[10] S. A. Moses *et al.*, A race-track trapped-ion quantum processor, Phys. Rev. X **13**, 041052 (2023).
[11] K. R. Brown, A. C. Wilson, Y. Colombe, C. Ospelkaus, A. M. Meier, E. Knill, D. Leibfried, and D. J. Wineland, Single-qubit-gate error below 10^{-4} in a trapped ion, Phys. Rev. A **84**, 030303(R) (2011).
[12] C. J. Ballance, T. P. Harty, N. M. Linke, M. A. Sepiol, and D. M. Lucas, High-fidelity quantum logic gates using trapped-ion hyperfine qubits, Phys. Rev. Lett. **117**, 060504 (2016).
[13] J. P. Gaebler, T. R. Tan, Y. Lin, Y. Wan, R. Bowler, A. C. Keith, S. Glancy, K. Coakley, E. Knill, D. Leibfried, and D. J. Wineland, High-fidelity universal gate set for $^{9}Be^{+}$ ion qubits, Phys. Rev. Lett. **117**, 060505 (2016).
[14] R. Srinivas, S. C. Burd, H. M. Knaack, R. T. Sutherland, A. Kwiatkowski, S. Glancy, E. Knill, D. J. Wineland, D. Leibfried, A. C. Wilson *et al.*, High-fidelity laser-free universal control of trapped ion qubits, Nature (London) **597**, 209 (2021).
[15] C. R. Clark, H. N. Tinkey, B. C. Sawyer, A. M. Meier, K. A. Burkhardt, C. M. Seck, C. M. Shappert, N. D. Guise, C. E. Volin, S. D. Fallek, H. T. Hayden, W. G. Rellergert, and K. R. Brown, High-fidelity Bell-state preparation with $^{40}Ca^{+}$ optical qubits, Phys. Rev. Lett. **127**, 130505 (2021).
[16] L. Egan, D. M. Debroy, C. Noel, A. Risinger, D. Zhu, D. Biswas, M. Newman, M. Li, K. R. Brown, M. Cetina, and C. Monroe, Fault-tolerant control of an error-corrected qubit, Nature (London) **598**, 281 (2021).
[17] L. Postler, S. Heußen, I. Pogorelov, M. Rispler, T. Feldker, M. Meth, C. D. Marciniak, R. Stricker, M. Ringbauer, R. Blatt, P. Schindler, M. Müller, and T. Monz, Demonstration of fault-tolerant universal quantum gate operations, Nature (London) **605**, 675 (2022).
[18] J.-S. Chen, E. Nielsen, M. Ebert, V. Inlek, K. Wright, V. Chaplin, A. Maksymov, E. Páez, A. Poudel, P. Maunz, and J. Gamble, Benchmarking a trapped-ion quantum computer with 29 algorithmic qubits, arXiv:2308.05071.

[19] S.-A. Guo, Y.-K. Wu, J. Ye, L. Zhang, W.-Q. Lian, R. Yao, Y. Wang, R.-Y. Yan, Y.-J. Yi, Y.-L. Xu *et al.*, A site-resolved 2D quantum simulator with hundreds of trapped ions under tunable couplings, arXiv:2311.17163.

[20] J. W. Britton, B. C. Sawyer, A. C. Keith, C.-C. J. Wang, J. K. Freericks, H. Uys, M. J. Biercuk, and J. J. Bollinger, Engineered two-dimensional Ising interactions in a trapped-ion quantum simulator with hundreds of spins, Nature (London) **484**, 489 (2012).

[21] J. G. Bohnet, B. C. Sawyer, J. W. Britton, M. L. Wall, A. M. Rey, M. Foss-Feig, and J. J. Bollinger, Quantum spin dynamics and entanglement generation with hundreds of trapped ions, Science **352**, 1297 (2016).

[22] A. Sørensen and K. Mølmer, Entanglement and quantum computation with ions in thermal motion, Phys. Rev. A **62**, 022311 (2000).

[23] G. Milburn, S. Schneider, and D. James, Ion trap quantum computing with warm ions, Fortschr. Phys. **48**, 801 (2000).

[24] D. J. Wineland, C. Monroe, W. M. Itano, D. Leibfried, B. E. King, and D. M. Meekhof, Experimental issues in coherent quantum-state manipulation of trapped atomic ions, J. Res. Natl. Inst. Stand. Technol. **103**, 259 (1998).

[25] D. Leibfried, R. Blatt, C. Monroe, and D. Wineland, Quantum dynamics of single trapped ions, Rev. Mod. Phys. **75**, 281 (2003).

[26] J.-S. Chen, K. Wright, N. C. Pisenti, D. Murphy, K. M. Beck, K. Landsman, J. M. Amini, and Y. Nam, Efficient-sideband-cooling protocol for long trapped-ion chains, Phys. Rev. A **102**, 043110 (2020).

[27] Q. Wu, Y. Shi, and J. Zhang, Continuous raman sideband cooling beyond the Lamb-Dicke regime in a trapped ion chain, Phys. Rev. Res. **5**, 023022 (2023).

[28] G. Birkl, J. A. Yeazell, R. Rückerl, and H. Walther, Polarization gradient cooling of trapped ions, Europhys. Lett. **27**, 197 (1994).

[29] S. Ejtemaee and P. C. Haljan, 3D sisyphus cooling of trapped ions, Phys. Rev. Lett. **119**, 043001 (2017).

[30] M. K. Joshi, A. Fabre, C. Maier, T. Brydges, D. Kiesenhofer, H. Hainzer, R. Blatt, and C. F. Roos, Polarization-gradient cooling of 1D and 2D ion Coulomb crystals, New J. Phys. **22**, 103013 (2020).

[31] J. Dalibard and C. Cohen-Tannoudji, Laser cooling below the Doppler limit by polarization gradients: Simple theoretical models, J. Opt. Soc. Am. B **6**, 2023 (1989).

[32] G. Morigi, J. Eschner, and C. H. Keitel, Ground state laser cooling using electromagnetically induced transparency, Phys. Rev. Lett. **85**, 4458 (2000).

[33] S.-L. Zhu, C. Monroe, and L.-M. Duan, Trapped ion quantum computation with transverse phonon modes, Phys. Rev. Lett. **97**, 050505 (2006).

[34] Y. Lin, J. P. Gaebler, T. R. Tan, R. Bowler, J. D. Jost, D. Leibfried, and D. J. Wineland, Sympathetic electromagnetically-induced-transparency laser cooling of motional modes in an ion chain, Phys. Rev. Lett. **110**, 153002 (2013).

[35] C. F. Roos, D. Leibfried, A. Mundt, F. Schmidt-Kaler, J. Eschner, and R. Blatt, Experimental demonstration of ground state laser cooling with electromagnetically induced transparency, Phys. Rev. Lett. **85**, 5547 (2000).

[36] J. Zhang, M.-C. Zhang, Y. Xie, C.-W. Wu, B.-Q. Ou, T. Chen, W.-S. Bao, P. Haljan, W. Wu, S. Zhang, and P.-X. Chen, Parallel electromagnetically induced transparency near ground-state cooling of a trapped-ion crystal, Phys. Rev. Appl. **18**, 014022 (2022).

[37] L. Feng, W. L. Tan, A. De, A. Menon, A. Chu, G. Pagano, and C. Monroe, Efficient ground-state cooling of large trapped-ion chains with an electromagnetically-induced-transparency tripod scheme, Phys. Rev. Lett. **125**, 053001 (2020).

[38] M. Qiao, Y. Wang, Z. Cai, B. Du, P. Wang, C. Luan, W. Chen, H.-R. Noh, and K. Kim, Double-electromagnetically-induced-transparency ground-state cooling of stationary two-dimensional ion crystals, Phys. Rev. Lett. **126**, 023604 (2021).

[39] E. Jordan, K. A. Gilmore, A. Shankar, A. Safavi-Naini, J. G. Bohnet, M. J. Holland, and J. J. Bollinger, Near ground-state cooling of two-dimensional trapped-ion crystals with more than 100 ions, Phys. Rev. Lett. **122**, 053603 (2019).

[40] P. J. Low, B. M. White, A. A. Cox, M. L. Day, and C. Senko, Practical trapped-ion protocols for universal qudit-based quantum computing, Phys. Rev. Res. **2**, 033128 (2020).

[41] J. Benhelm, G. Kirchmair, C. F. Roos, and R. Blatt, Experimental quantum-information processing with $^{43}Ca^{+}$ ions, Phys. Rev. A **77**, 062306 (2008).

[42] T. R. Tan, J. P. Gaebler, Y. Lin, Y. Wan, R. Bowler, D. Leibfried, and D. J. Wineland, Multi-element logic gates for trapped-ion qubits, Nature (London) **528**, 380 (2015).

[43] M. R. Dietrich, N. Kurz, T. Noel, G. Shu, and B. B. Blinov, Hyperfine and optical barium ion qubits, Phys. Rev. A **81**, 052328 (2010).

[44] S. X. Wang, G. Hao Low, N. S. Lachenmyer, Y. Ge, P. F. Herskind, and I. L. Chuang, Laser-induced charging of microfabricated ion traps, J. Appl. Phys. **110**, 104901 (2011).

[45] See Supplemental Material at http://link.aps.org/supplemental/10.1103/PhysRevLett.133.113204 for details about our numerical simulation method, the way to calibrate Rabi rates of different laser beams, the optimization of EIT cooling parameters, the way to engineer the Fano-like spectrum for simultaneous cooling of different phonon modes, and generalizing our scheme to higher-nuclear-spin ions, which includes Ref. [46].

[46] N. Scharnhorst, J. Cerrillo, J. Kramer, I. D. Leroux, J. B. Wübbena, A. Retzker, and P. O. Schmidt, Experimental and theoretical investigation of a multimode cooling scheme using multiple electromagnetically-induced-transparency resonances, Phys. Rev. A **98**, 023424 (2018).

[47] K. J. Arnold, S. R. Chanu, R. Kaewuam, T. R. Tan, L. Yeo, Z. Zhang, M. S. Safronova, and M. D. Barrett, Measurements of the branching ratios for $6P_{1/2}$ decays in $^{138}Ba^{+}$, Phys. Rev. A **100**, 032503 (2019).